

# Supplementary Information for ‘Probing “hydridic hydrogen bonds” using energy decomposition analysis based on absolutely localized molecular orbitals’

David W. Roberts<sup>a</sup> and Yuezhi Mao<sup>\*a</sup>

## CONTENTS

<b>S1 Brief overview of the ALMO-EDA methods</b>	<b>2</b>
S1.1 The second-generation ALMO-EDA methods . . . . .	2
S1.2 Adiabatic ALMO-EDA . . . . .	3
<b>S2 Computational details</b>	<b>4</b>
<b>S3 Additional tables and figures</b>	<b>5</b>

---

<sup>a</sup> Department of Chemistry and Biochemistry, San Diego State University, San Diego, CA 92182, USA; E-mail: ymao2@sdsu.edu

# S1 Brief overview of the ALMO-EDA methods

## S1.1 The second-generation ALMO-EDA methods

The second-generation absolutely localized molecular orbital energy decomposition analysis (ALMO-EDA-II)<sup>1-3</sup> partitions the total intermolecular interaction energy ( $\Delta E_{\text{INT}}$ ) evaluated using Kohn-Sham density functional theory (KS-DFT) into five components: permanent electrostatics (ELEC), Pauli repulsion (PAULI), dispersion (DISP), polarization (POL), and charge transfer (CT):

$$\Delta E_{\text{INT}} = \Delta E_{\text{ELEC}} + \Delta E_{\text{PAULI}} + \Delta E_{\text{DISP}} + \Delta E_{\text{POL}} + \Delta E_{\text{CT}}. \quad (\text{S1})$$

This decomposition is achieved by defining two intermediate states connecting the initial (isolated fragments) and final (fully relaxed complex) states in the formation of an intermolecular complex:<sup>4</sup> (i) the frozen (Frz) state, where the fragments interact with each other under the geometry of the final complex but their electronic structures (KS orbitals) remain the same as in isolation; (ii) the polarized (Pol) state, on which the fragment orbitals are allowed to relax in the presence of other fragments while inter-fragment orbital mixing remains forbidden. The energy difference between the Frz state and the sum of the isolated fragment energies ( $\{E_A\}$ ) is defined as the frozen interaction energy ( $\Delta E_{\text{FRZ}}$ ):

$$\Delta E_{\text{FRZ}} = E_{\text{Frz}} - \sum_{A=1}^{N_{\text{frag}}} E_A, \quad (\text{S2})$$

and the polarization and charge-transfer contributions are defined in a similar manner:

$$\Delta E_{\text{POL}} = E_{\text{Pol}} - E_{\text{Frz}} \quad (\text{S3})$$

$$\Delta E_{\text{CT}} = E_{\text{Full}} - E_{\text{Pol}} \quad (\text{S4})$$

where  $E_{\text{Pol}}$  is the energy of the polarized state and  $E_{\text{Full}}$  is the KS-DFT energy of the fully relaxed intermolecular complex.

To obtain the 5-term decomposition as given by Eq. (S1), we need to further decompose the frozen interaction into the ELEC, PAULI, and DISP contributions:

$$\Delta E_{\text{FRZ}} = \Delta E_{\text{ELEC}} + \Delta E_{\text{PAULI}} + \Delta E_{\text{DISP}} \quad (\text{S5})$$

This can be achieved by using either the ‘‘quasiclassical’’<sup>5</sup> or ‘‘orthogonal’’<sup>6</sup> decomposition schemes. Since the latter method has not been made compatible with calculations involving effective core potentials (which is needed for iodine) yet, in this work we employed the ‘‘quasiclassical’’ decomposition scheme exclusively. Under this scheme, the permanent electrostatic interaction between fragments is simply defined as the Coulomb interaction between the charge densities of isolated fragments (including both electrons and nuclei):

$$\Delta E_{\text{ELEC}} = \sum_{A < B} \int \int \rho_A^{\text{tot}}(\mathbf{r}_1) \frac{1}{|\mathbf{r}_1 - \mathbf{r}_2|} \rho_B^{\text{tot}}(\mathbf{r}_2) d\mathbf{r}_1 d\mathbf{r}_2 \quad (\text{S6})$$

The definition of the DISP term requires an auxiliary ‘‘dispersion-free’’ exchange-correlation (DFXC) functional in company with the primary functional:

$$\Delta E_{\text{DISP}} = \left( E_{\text{XC}}[\mathbf{P}_{\text{FRZ}}] - \sum_{A=1}^{N_{\text{frag}}} E_{\text{XC}}[\mathbf{P}_A] \right) - \left( E_{\text{DFXC}}[\mathbf{P}_{\text{FRZ}}] - \sum_{A=1}^{N_{\text{frag}}} E_{\text{DFXC}}[\mathbf{P}_A] \right), \quad (\text{S7})$$

where  $E_{\text{XC}}$  and  $E_{\text{DFXC}}$  are the exchange-correlation energy calculated using the primary and the ‘‘dispersion-free’’ XC functional, respectively,  $\mathbf{P}_{\text{FRZ}}$  is the one-particle density matrix (1PDM) for the frozen state, and  $\mathbf{P}_A$ ’s are the 1PDMs for the isolated fragments. In this work, we employed the Hartree-Fock ‘‘exchange functional’’ as the DFXC method, which was shown to give reliable results for dispersion-corrected hybrid functionals such as  $\omega\text{B97X-V}$ .<sup>7</sup> Finally, with  $\Delta E_{\text{ELEC}}$  and  $\Delta E_{\text{DISP}}$  both defined, the remainder of  $\Delta E_{\text{FRZ}}$  is defined as  $\Delta E_{\text{PAULI}}$ .

Deeper insights into the polarization and charge-transfer terms can be obtained using the recently developed non-perturbative polarization and charge-transfer analysis.<sup>8,9</sup> Compared to the previously developed perturbative ALMO-based charge-transfer analysis,<sup>10</sup> the non-perturbative approach has the advantage that the energetic contributions from the forward and backward donations are almost exactly fragment-pairwise additive such that the undesirable higher-order term (which cannot be further partitioned) can be ignored:<sup>9</sup>

$$\Delta E_{\text{CT}} = \sum_{A < B}^{N_{\text{frag}}} \Delta E_{\text{CT}}^{A \rightarrow B} + \Delta E_{\text{CT}}^{B \rightarrow A} \quad (\text{S8})$$

Similarly, the total polarization energy can be partitioned into exactly fragment-wise additive contributions:<sup>8</sup>

$$\Delta E_{\text{POL}} = \sum_{A=1}^{N_{\text{frag}}} \Delta E_{\text{POL}}^A \quad (\text{S9})$$

We refer the reader to Refs. 8 and 9 for the mathematical details involved in these analysis schemes, including the definition of the complementary occupied-virtual pairs (COVPs).

## S1.2 Adiabatic ALMO-EDA

The ALMO-EDA-II scheme recapitulated above can be referred to as a *vertical* EDA scheme because all the terms are calculated within the same geometry (typically the fully relaxed structure of the complex). To decompose the shifts in structural and vibrational features induced by interactions between molecules, the ALMO-EDA method has been reformulated to adopt an *adiabatic* picture,<sup>11</sup> in which the complex geometry is relaxed on the potential energy surfaces (PESs) associated with the frozen (Frz), polarized (Pol), and fully relaxed (Full) states as defined in ALMO-EDA. The harmonic frequencies can then be calculated at the optimized structure on each surface. In this way, the shift in the frequency of a vibrational mode upon the complex formation ( $\Delta\nu_{\text{total}}$ ) can be partitioned into frozen (FRZ), polarization (POL), and charge transfer (CT) contributions, which is in the same fashion as the decomposition of interaction energy, except that the frozen contribution cannot be further partitioned within the current adiabatic EDA framework:

$$\Delta\nu_{\text{total}} = \Delta\nu_{\text{FRZ}} + \Delta\nu_{\text{POL}} + \Delta\nu_{\text{CT}} \quad (\text{S10})$$

$$\Delta\nu_{\text{FRZ}} = \nu_{\text{Frz}} - \nu_{\text{Iso}}, \quad \Delta\nu_{\text{POL}} = \nu_{\text{Pol}} - \nu_{\text{Frz}}, \quad \Delta\nu_{\text{CT}} = \nu_{\text{Full}} - \nu_{\text{Pol}}, \quad (\text{S11})$$

where  $\nu_{\text{Iso}}$ ,  $\nu_{\text{Frz}}$ ,  $\nu_{\text{Pol}}$ , and  $\nu_{\text{Full}}$  stand for harmonic frequencies calculated at the optimized geometries in the isolated fragment, frozen, polarized, and fully relaxed states, respectively. We note that the FRZ, POL, and CT contributions to the vibrational frequency shift,  $\Delta\nu_{\text{FRZ}}$ ,  $\Delta\nu_{\text{POL}}$ , and  $\Delta\nu_{\text{CT}}$ , are not necessarily proportional to the magnitudes of the corresponding energy components, since different energy components would have different impacts on the vibrational frequency of an oscillator, which is closely related to its force constant, the second derivatives of potential energy with respect to nuclear positions.

The adiabatic ALMO-EDA scheme was further extended to include two additional intermediate states between the Pol and Full states, on which only one direction of CT (either forward or backward) is allowed.<sup>12</sup> These two intermediate states, which are referred to as the ‘‘CTf’’ and ‘‘CTb’’ states (‘‘f/b’’ for forward/backward), are variationally optimized based on the generalized self-consistent field for molecular interaction (SCF-MI)<sup>12,13</sup> scheme. One can thus readily optimize the complex structure on the CTf/CTb surface and calculate the harmonic frequencies. The vibrational frequency shifts owing to the forward/backward CT can thus be obtained as

$$\Delta\nu_{\text{CTf}} = \nu_{\text{CTf}} - \nu_{\text{Pol}} \quad (\text{S12})$$

$$\Delta\nu_{\text{CTb}} = \nu_{\text{CTb}} - \nu_{\text{Pol}} \quad (\text{S13})$$

## S2 Computational details

All electronic structure calculations were performed using the Q-Chem 6.1 software package<sup>14</sup>, and the IQmol software was employed to visualize the geometries, molecular orbitals, and electrostatic potential (ESP) maps. The ALMO-EDA-II<sup>1,3</sup> calculations were performed at complex geometries optimized at the  $\omega$ B97X-V<sup>7</sup>/def2-SVPD<sup>15,16</sup> level, which are exactly the same geometries as those optimized on the “Full” surface in the adiabatic EDA calculations. The geometry optimizations were set to converge when the maximum component of the nuclear gradient is below  $5.0 \times 10^{-5}$  a.u. and the energy change from the previous iteration is below  $10^{-7}$  a.u. A larger basis set (def2-TZVPPD<sup>15,16</sup>) was then employed for the EDA calculations. The effective core potential associated with the Karlsruhe “def2” basis sets was applied to iodine. For the numerical integration involved in DFT calculations, a (99, 590) grid (99 radial shells with 590 Lebedev points in each) was used for the exchange-correlation functional, and the SG-1 grid<sup>17</sup> was used for the VV10<sup>18</sup> non-local correlation functional for dispersion correction. Additional ALMO-EDA calculations were performed (i) using the B3LYP<sup>19</sup> functional with Grimme’s D3 correction with Becke-Johnson damping<sup>20</sup> (denoted as “B3LYP-D3(BJ)”), as well as the  $\omega$ B97X-D3(BJ) functional<sup>21</sup> which shares same parent XC functional as  $\omega$ B97X-V, and (ii) using the geometries supplied in Ref. 22, which were optimized at the RI-MP2/cc-pwCVTZ<sup>23</sup> level. The results for (i) and (ii) are summarized in Tables S2 and S3, respectively, which reflect the same trends as the primary set of results (Table S1) that we report in the main paper.

As mentioned in Sec. S1 above, the decomposition of the frozen interaction energy utilizes the “quasiclassical” scheme<sup>5,6</sup> (with Q-Chem keywords `EDA_CLS_ELEC` and `EDA_CLS_DISP` both set to `TRUE`), for which the Hartree-Fock theory was chosen to be the DFXC functional (Q-Chem default). The fragment electrical response function (FERF) method<sup>13</sup> was employed to calculate the polarization energy. The non-perturbative polarization and charge-transfer analyses<sup>8,9</sup> were performed together with the ALMO-EDA-II calculations by setting both `EDA_POL_A` and `EDA_VCT_A` to `TRUE`, and the dominant complementary occupied-virtual pairs (COVPs) in the polarization and charge-transfer processes were obtained and visualized.

For the adiabatic ALMO-EDA<sup>11</sup> calculation, the geometry of the H-bond complexes were optimized on the frozen (Frz), polarized (Pol), and fully relaxed (Full) surfaces at the  $\omega$ B97X-V/def2-SVPD level, which was followed by a harmonic frequency calculation at the optimized geometry on each surface. We note that since the adiabatic EDA employs the original ALMO definition for the Pol state (nuclear gradients for the FERG-based  $E_{\text{Pol}}$  are unavailable),<sup>4,24</sup> a smaller basis set was used for the adiabatic EDA calculations to avoid potential contamination of polarization (intra-fragment orbital mixing) by charge transfer (inter-fragment orbital mixing). Due to the lack of analytical hessian for the Frz and Pol states, the frequencies were calculated using a finite-difference method based on nuclear gradients (which are available for all three surfaces). The resulting harmonic frequencies were scaled by a factor of 0.954, which was fitted based on the results of  $\omega$ B97X-V with the def2-TZVP basis on a recently compiled vibrational frequency dataset.<sup>25</sup> The application of this scaling factor to the vibrational frequency of the  $\text{Me}_3\text{SiH}$  monomer yields  $\nu_{\text{SiH}} = 2107.0 \text{ cm}^{-1}$ , which is in excellent agreement with the experimental value (2109  $\text{cm}^{-1}$ ) measured in Ar matrix.<sup>22</sup> The vibrational forward-backward (VFB) analysis was performed for a selected set of complexes, for which the same procedure as described above was applied to the two additional intermediate surfaces, CTf and CTb.

The forces arising from the frozen interaction components were calculated using a 5-point stencil: starting from the optimized structure of a complex on the *frozen* surface, we performed ALMO-EDA-II calculations (focusing on the results of  $\Delta E_{\text{ELEC}}$ ,  $\Delta E_{\text{PAULI}}$ , and  $\Delta E_{\text{DISP}}$ ) with the X–H bond length modified by  $\pm 0.0005$  and  $\pm 0.001$  Å. The forces along the X→H direction arising from component  $\alpha$  can then be evaluated based on

$$f_{\text{X}\rightarrow\text{H}} = \frac{\Delta E_{\alpha}(x + 2\Delta x) - 8\Delta E_{\alpha}(x + \Delta x) + 8\Delta E_{\alpha}(x - \Delta x) - \Delta E_{\alpha}(x - 2\Delta x)}{12\Delta x} \quad (\text{S1})$$

where  $\alpha = \text{ELEC}$ ,  $\text{PAULI}$ , or  $\text{DISP}$ , and  $\Delta x = 0.0005$  Å. We note that the forces arising from the three components do not add up to zero as they compensate for the forces due to the distortion from monomer geometry, i.e., the elongation or contraction of the X–H bond.

### S3 Additional tables and figures

Table S1: ALMO-EDA-II results (in kJ/mol) for the prototypical protonic and hydridic hydrogen-bond (HB) complexes investigated in this work. The calculations were performed at the  $\omega$ B97X-V/def2-TZVPPD level using geometries optimized with  $\omega$ B97X-V/def2-SVPD.

System	ELEC	PAULI	DISP	POL	CT	Total
H <sub>2</sub> O dimer	-35.13	32.70	-6.40	-4.83	-7.62	-21.28
CF <sub>3</sub> H...H <sub>2</sub> O	-21.61	17.97	-5.33	-2.87	-3.09	-14.93
Me <sub>3</sub> SiH...ICN	-21.50	36.73	-16.23	-5.83	-9.39	-16.21
Me <sub>3</sub> SiH...BrCN	-12.01	20.88	-12.62	-2.72	-4.48	-10.95
Me <sub>3</sub> SiH...ICF <sub>3</sub>	-13.61	24.99	-14.98	-2.86	-5.35	-11.81
Me <sub>3</sub> SiH...COF <sub>2</sub>	-13.34	20.81	-15.23	-2.15	-2.84	-12.75
Me <sub>3</sub> SiH...NO <sub>2</sub> F	-11.07	18.01	-14.41	-1.37	-1.76	-10.60
Me <sub>3</sub> SiH...HCN	-9.88	15.01	-11.94	-1.64	-1.68	-10.13
Me <sub>3</sub> SiH...K <sup>+</sup>	-35.10	23.19	-5.59	-26.45	-3.85	-47.80

Table S2: ALMO-EDA-II results (in kJ/mol) for the prototypical protonic and hydridic HB complexes investigated in this work obtained using (i) B3LYP-D3(BJ) and (ii)  $\omega$ B97X-D3(BJ) functionals with the def2-TZVPPD basis set. All calculations were performed on geometries optimized at the  $\omega$ B97X-V/def2-SVPD level.

System	B3LYP-D3(BJ)/def2-TZVPPD					
	ELEC	PAULI	DISP	POL	CT	Total
H <sub>2</sub> O dimer	-35.20	33.59	-6.84	-4.81	-8.63	-21.89
CF <sub>3</sub> H...H <sub>2</sub> O	-21.55	18.41	-5.40	-2.84	-3.65	-15.04
Me <sub>3</sub> SiH...ICN	-21.98	37.79	-18.96	-5.44	-12.48	-21.07
Me <sub>3</sub> SiH...BrCN	-12.12	21.39	-14.52	-2.49	-6.17	-13.92
Me <sub>3</sub> SiH...ICF <sub>3</sub>	-13.99	25.78	-17.14	-2.52	-7.40	-15.27
Me <sub>3</sub> SiH...COF <sub>2</sub>	-13.39	21.42	-14.69	-1.95	-3.76	-12.37
Me <sub>3</sub> SiH...NO <sub>2</sub> F	-11.28	18.54	-13.03	-1.18	-2.33	-9.27
Me <sub>3</sub> SiH...HCN	-9.86	15.45	-12.71	-1.49	-2.43	-11.04
Me <sub>3</sub> SiH...K <sup>+</sup>	-35.52	24.04	-11.89	-27.36	-4.51	-55.24
System	$\omega$ B97X-D3(BJ)/def2-TZVPPD					
	ELEC	PAULI	DISP	POL	CT	Total
H <sub>2</sub> O dimer	-35.09	32.70	-6.07	-4.80	-7.60	-20.86
CF <sub>3</sub> H...H <sub>2</sub> O	-21.59	17.98	-4.95	-2.85	-3.07	-14.50
Me <sub>3</sub> SiH...ICN	-21.35	36.6	-20.90	-5.52	-9.31	-20.48
Me <sub>3</sub> SiH...BrCN	-11.89	20.80	-15.58	-2.51	-4.44	-13.61
Me <sub>3</sub> SiH...ICF <sub>3</sub>	-13.49	24.89	-18.62	-2.62	-5.29	-15.12
Me <sub>3</sub> SiH...COF <sub>2</sub>	-13.23	20.71	-15.60	-1.96	-2.81	-12.88
Me <sub>3</sub> SiH...NO <sub>2</sub> F	-10.98	17.93	-13.74	-1.20	-1.73	-9.73
Me <sub>3</sub> SiH...HCN	-9.82	14.97	-13.30	-1.54	-1.66	-11.34
Me <sub>3</sub> SiH...K <sup>+</sup>	-35.13	23.19	-12.28	-26.13	-3.84	-54.20

Table S3: ALMO-EDA-II results (in kJ/mol) for the hydridic HB complexes investigated in this work. The calculations were performed at the  $\omega$ B97X-V/def2-TZVPPD level using the geometries obtained from the SI of Ref. 22 (optimized using RI-MP2/cc-pwCVTZ).

System	ELEC	PAULI	DISP	POL	CT	Total
Me <sub>3</sub> SiH...ICN	-18.91	31.30	-15.01	-5.18	-7.89	-15.68
Me <sub>3</sub> SiH...BrCN	-14.60	26.19	-13.41	-3.14	-5.70	-10.66
Me <sub>3</sub> SiH...ICF <sub>3</sub>	-15.00	28.05	-15.68	-3.08	-5.88	-11.58
Me <sub>3</sub> SiH...COF <sub>2</sub>	-12.82	19.27	-14.49	-2.07	-2.70	-12.80
Me <sub>3</sub> SiH...NO <sub>2</sub> F	-12.38	19.09	-14.76	-1.60	-1.87	-11.52
Me <sub>3</sub> SiH...HCN	-10.37	16.17	-12.33	-1.69	-1.82	-10.04
Me <sub>3</sub> SiH...K <sup>+</sup>	-30.28	15.19	-4.48	-24.05	-2.80	-46.42

Table S4: ALMO-EDA-II results (in kJ/mol) for the additional protonic HB complexes included in Table 1 in the main text: (i) *t*-BuOH with H<sub>2</sub>O, ICN, COF<sub>2</sub>, and HCN; (ii) H<sub>2</sub>S...H<sub>2</sub>O; and (iii) *t*-BuSH with H<sub>2</sub>O, ICN, COF<sub>2</sub>, and HCN. The calculations were performed at the  $\omega$ B97X-V/def2-TZVPPD //  $\omega$ B97X-V/def2-SVPD level of theory. For each complex, the chemical species before and after the “...” correspond to the proton donor and acceptor, respectively.

System	ELEC	PAULI	DISP	POL	CT	Total
<i>t</i> -BuOH...OH <sub>2</sub>	-34.85	36.17	-10.31	-5.51	-7.33	-21.83
<i>t</i> -BuOH...ICN	-24.62	27.18	-10.74	-4.78	-5.54	-18.49
<i>t</i> -BuOH...COF <sub>2</sub>	-17.18	19.70	-8.91	-3.13	-3.52	-13.04
<i>t</i> -BuOH...HCN	-23.60	25.20	-9.83	-4.20	-5.17	-17.60
HSH...OH <sub>2</sub>	-18.04	19.36	-6.04	-2.81	-3.76	-11.29
<i>t</i> -BuSH...OH <sub>2</sub>	-16.32	19.70	-9.91	-2.61	-2.97	-12.12
<i>t</i> -BuSH...ICN	-12.55	16.94	-10.49	-2.53	-2.53	-11.16
<i>t</i> -BuSH...COF <sub>2</sub>	-8.32	12.45	-9.58	-1.18	-1.59	-8.22
<i>t</i> -BuSH...HCN	-11.74	15.75	-9.88	-2.26	-2.26	-10.39

Table S5: Comparison of ALMO-EDA results calculated using B3LYP-D3(BJ) and the plain B3LYP functional for three hydridic HB complexes. The results for “B3LYP-D3(BJ)” and “B3LYP” were calculated using the same geometries as in the main manuscript (optimized using  $\omega$ B97X-V/def2-SVPD), whereas the “B3LYP//B3LYP” results were calculated using geometries reoptimized at the B3LYP/def2-SVPD level.

System	Method	ELEC	PAULI	DISP	POL	CT	Total
Me <sub>3</sub> SiH...ICN	B3LYP-D3(BJ)	-21.98	37.79	-18.96	-5.44	-12.48	-21.07
	B3LYP	-21.98	37.79	-4.23	-5.44	-12.48	-6.35
	B3LYP//B3LYP	-20.41	32.89	-4.02	-4.74	-13.21	-9.50
Me <sub>3</sub> SiH...COF <sub>2</sub>	B3LYP-D3(BJ)	-13.39	21.42	-14.69	-1.95	-3.76	-12.37
	B3LYP	-13.39	21.42	-2.39	-1.95	-3.76	-0.07
	B3LYP//B3LYP	-8.32	9.80	-0.82	-1.23	-2.19	-2.76
Me <sub>3</sub> SiH...HCN	B3LYP-D3(BJ)	-9.86	15.45	-12.71	-1.49	-2.43	-11.04
	B3LYP	-9.86	15.45	-2.30	-1.49	-2.43	-0.62
	B3LYP//B3LYP	-8.46	10.85	-1.76	-2.38	-4.43	-6.19

Table S6: Adiabatic ALMO-EDA results for protonic and hydridic HB complexes investigated in this work at the  $\omega$ B97X-V/def2-SVPD level. The X–H bond lengths ( $r_{\text{XH}}$ , in Å) and stretching frequencies ( $\nu_{\text{XH}}$ , in  $\text{cm}^{-1}$ ) calculated on the frozen, polarized, and fully relaxed surfaces are reported.<sup>a</sup> A scaling factor 0.954 was applied to the harmonic frequencies. For the water dimer, the frequency of the symmetric O–H stretch of the proton-donor  $\text{H}_2\text{O}$  is reported.

System	Frozen		Polarized		Fully relaxed	
	$r_{\text{XH}}$ (Å)	$\nu_{\text{XH}}$ ( $\text{cm}^{-1}$ )	$r_{\text{XH}}$ (Å)	$\nu_{\text{XH}}$ ( $\text{cm}^{-1}$ )	$r_{\text{XH}}$ (Å)	$\nu_{\text{XH}}$ ( $\text{cm}^{-1}$ )
$\text{HOH} \cdots \text{OH}_2$	0.96386	3693.4	0.96501	3686.1	0.97012	3587.4
$\text{CF}_3\text{H} \cdots \text{H}_2\text{O}$	1.09740	3069.5	1.09743	3067.9	1.09843	3048.1
$\text{Me}_3\text{SiH} \cdots \text{ICN}$	1.50567	2078.7	1.50695	2072.9	1.51164	2044.4
$\text{Me}_3\text{SiH} \cdots \text{BrCN}$	1.50431	2085.6	1.50508	2081.0	1.50722	2067.1
$\text{Me}_3\text{SiH} \cdots \text{ICF}_3$	1.50371	2088.6	1.50446	2084.8	1.50728	2064.3
$\text{Me}_3\text{SiH} \cdots \text{COF}_2$	1.50387	2088.0	1.50441	2087.0	1.50502	2082.7
$\text{Me}_3\text{SiH} \cdots \text{NO}_2\text{F}$	1.50291	2095.0	1.50325	2094.6	1.50276	2097.4
$\text{Me}_3\text{SiH} \cdots \text{HCN}$	1.50390	2086.0	1.50459	2082.2	1.50498	2079.4
$\text{Me}_3\text{SiH} \cdots \text{K}^+$	1.52215	2008.8	1.53193	1992.6	1.53337	1995.6

<sup>a</sup> Bond lengths and scaled harmonic frequencies for the monomers:  $\text{H}_2\text{O}$ :  $r_{\text{OH}} = 0.96255$  Å,  $\nu_{\text{OH}} = 3695.5$   $\text{cm}^{-1}$ ;  $\text{CF}_3\text{H}$ :  $r_{\text{CH}} = 1.09998$  Å,  $\nu_{\text{CH}} = 3023.3$   $\text{cm}^{-1}$ ;  $\text{Me}_3\text{SiH}$ :  $r_{\text{SiH}} = 1.49988$  Å,  $\nu_{\text{OH}} = 2107.0$   $\text{cm}^{-1}$ .

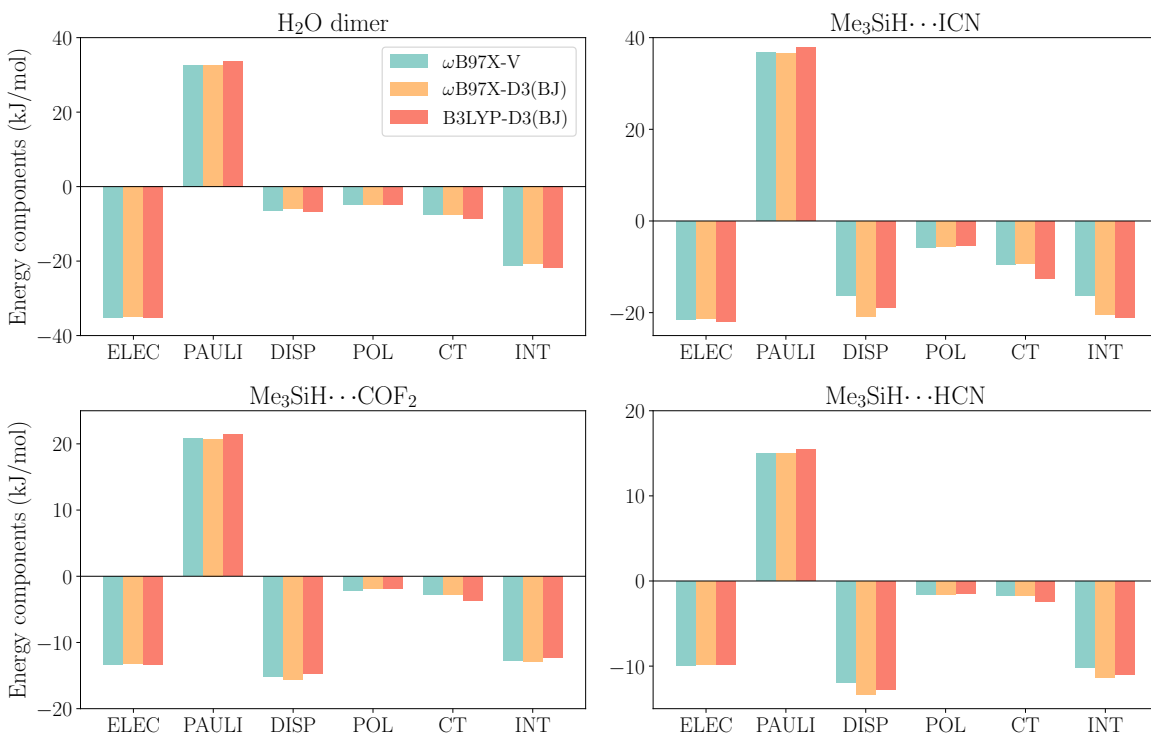


Figure S1: Comparison of the ALMO-EDA-II results obtained using the  $\omega$ B97X-V,  $\omega$ B97X-D3(BJ), and B3LYP-D3(BJ) functionals for (i) the  $\text{H}_2\text{O}$  dimer; (ii)  $\text{Me}_3\text{SiH} \cdots \text{ICN}$ ; (iii)  $\text{Me}_3\text{SiH} \cdots \text{COF}_2$ ; and (iv)  $\text{Me}_3\text{SiH} \cdots \text{HCN}$ . The def2-TZVPPD basis set was used for all the calculations.

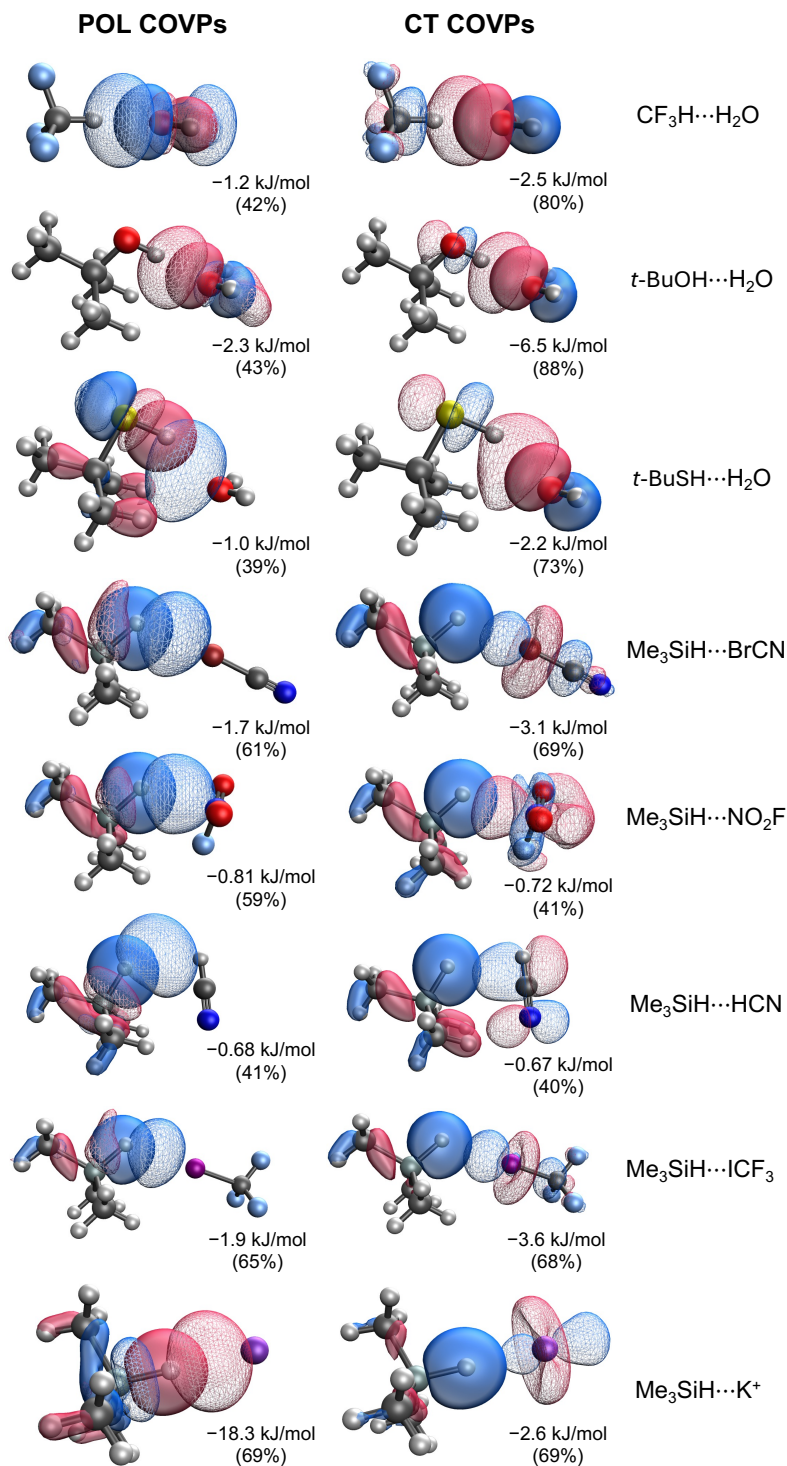


Figure S2: Dominant complementary occupied-virtual pairs (COVPs) for polarization and charge transfer of additional protonic and hydric HB complexes investigated in this work. Within each pair, the solid and meshed contour surfaces represent the occupied and virtual orbitals, respectively. The energetic contribution associated with each COVP is reported in kJ/mol, with its percentage contribution to the total POL or CT energy shown in the parentheses. The COVPs were generated from ALMO-based POL and CT analyses at the  $\omega\text{B97X-V}/\text{def2-TZVPPD}$  level and plotted using a contour isovalue of  $0.04 \text{ \AA}^{-3}$ .

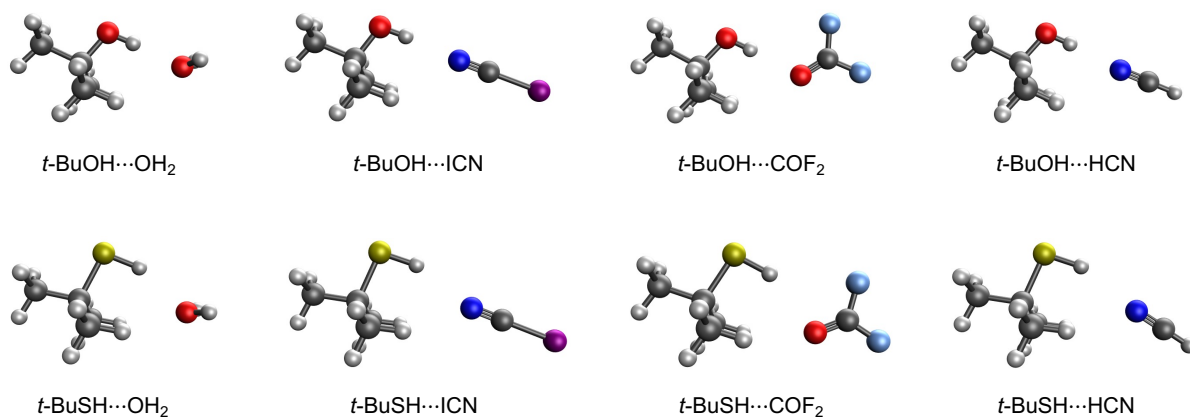


Figure S3: Optimized geometries (at the  $\omega\text{B97X-V/def2-SVPD}$  level) of the  $t\text{-BuOH}$  and  $t\text{-BuSH}$  complexes with  $\text{H}_2\text{O}$ ,  $\text{ICN}$ ,  $\text{COF}_2$ , and  $\text{HCN}$ .

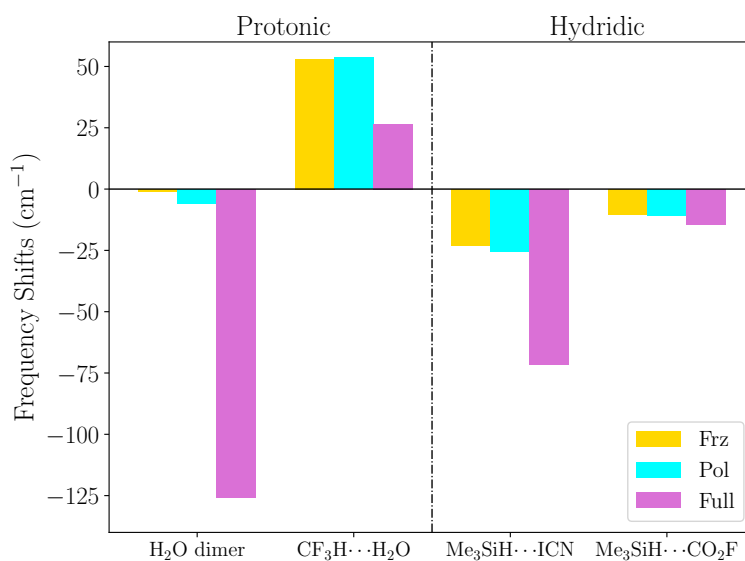


Figure S4: Adiabatic EDA results calculated using  $\text{B3LYP-D3(BJ)/def2-SVPD}$ . The calculated harmonic frequencies were scaled by a factor of 0.964.<sup>25</sup> The other details are the same as in Fig. 3 of the main paper.

## References

- 1 P. R. Horn, Y. Mao and M. Head-Gordon, *Phys. Chem. Chem. Phys.*, 2016, **18**, 23067–23079.
- 2 Y. Mao, D. S. Levine, M. Loipersberger, P. R. Horn and M. Head-Gordon, *Phys. Chem. Chem. Phys.*, 2020, **22**, 12867–12885.
- 3 Y. Mao, M. Loipersberger, P. R. Horn, A. Das, O. Demerdash, D. S. Levine, S. Prasad Veccham, T. Head-Gordon and M. Head-Gordon, *Annu. Rev. Phys. Chem.*, 2021, **72**, 641–666.
- 4 R. Z. Khaliullin, E. A. Cobar, R. C. Lochan, A. T. Bell and M. Head-Gordon, *J. Phys. Chem. A*, 2007, **111**, 8753–8765.
- 5 Y. Mao, O. Demerdash, M. Head-Gordon and T. Head-Gordon, *J. Chem. Theory Comput.*, 2016, **12**, 5422–5437.
- 6 P. R. Horn, Y. Mao and M. Head-Gordon, *J. Chem. Phys.*, 2016, **144**, 114107.
- 7 N. Mardirossian and M. Head-Gordon, *Phys. Chem. Chem. Phys.*, 2014, **16**, 9904–9924.
- 8 H. Shen, S. P. Veccham and M. Head-Gordon, *J. Chem. Theory Comput.*, 2023, **19**, 8624–8638.
- 9 S. P. Veccham, J. Lee, Y. Mao, P. R. Horn and M. Head-Gordon, *Phys. Chem. Chem. Phys.*, 2021, **23**, 928–943.
- 10 R. Z. Khaliullin, A. T. Bell and M. Head-Gordon, *J. Chem. Phys.*, 2008, **128**, 184112.
- 11 Y. Mao, P. R. Horn and M. Head-Gordon, *Phys. Chem. Chem. Phys.*, 2017, **19**, 5944–5958.
- 12 M. Loipersberger, Y. Mao and M. Head-Gordon, *J. Chem. Theory Comput.*, 2020, **16**, 1073–1089.
- 13 P. R. Horn and M. Head-Gordon, *J. Chem. Phys.*, 2015, **143**, 114111.
- 14 E. Epifanovsky, A. T. Gilbert, X. Feng, J. Lee, Y. Mao, N. Mardirossian, P. Pokhilko, A. F. White, M. P. Coons, A. L. Dempwolff *et al.*, *J. Chem. Phys.*, 2021, **155**, 084801.
- 15 F. Weigend and R. Ahlrichs, *Phys. Chem. Chem. Phys.*, 2005, **7**, 3297–3305.
- 16 D. Rappoport and F. Furche, *J. Chem. Phys.*, 2010, **133**, 134105.
- 17 P. M. Gill, B. G. Johnson and J. A. Pople, *Chem. Phys. Lett.*, 1993, **209**, 506–512.
- 18 O. A. Vydrov and T. Van Voorhis, *J. Chem. Phys.*, 2010, **133**, 244103.
- 19 A. D. Becke, *J. Chem. Phys.*, 1993, **98**, 5648–5652.
- 20 S. Grimme, S. Ehrlich and L. Goerigk, *J. Comput. Chem.*, 2011, **32**, 1456–1465.
- 21 A. Najibi and L. Goerigk, *J. Chem. Theory Comput.*, 2018, **14**, 5725–5738.
- 22 S. Civiš, M. Lamanec, V. Špirko, J. Kubišta, M. Špet’ko and P. Hobza, *J. Am. Chem. Soc.*, 2023, **145**, 8550–8559.
- 23 K. A. Peterson and T. H. Dunning Jr, *J. Chem. Phys.*, 2002, **117**, 10548–10560.
- 24 R. Z. Khaliullin, M. Head-Gordon and A. T. Bell, *J. Chem. Phys.*, 2006, **124**, 204105.
- 25 J. Liang, X. Feng, X. Liu and M. Head-Gordon, *J. Chem. Phys.*, 2023, **158**, 204109.